Adsorptive removal of methyl orange from aqueous solution with metal-organic frameworks, porous chromium-benzenedicarboxylates

Enamul Haque[a], Ji Eun Lee[a], In Tae Jang[b], Young Kyu Hwang[b], Jong-San Chang[b], Jonggeon Jegal[c], Sung Hwa Jhung[a],*

[a] Department of Chemistry, Kyungpook National University, Daegu 702-701, Republic of Korea
[b] Research Center for Nanocatalysts, Korea Research Institute of Chemical Technology, P.O. Box, 107, Yusung, Daejeon 305-600, Republic of Korea
[c] Membrane and Separation Research Center, Korea Research Institute of Chemical Technology, P.O. Box 107, Yusung, Daejeon 305-600, Republic of Korea

ARTICLE INFO

ABSTRACT

Two typical highly porous metal-organic framework (MOF) materials based on chromium-benzenedicarboxylates (Cr-BDC) obtained from Material of Institute Lavoisier with special structure of MIL-101 and MIL-53 have been used for the adsorptive removal of methyl orange (MO), a harmful anionic dye, from aqueous solutions. The adsorption capacity and adsorption kinetic constant of MIL-101 are greater than those of MIL-53, showing the importance of porosity and pore size for the adsorption. The performance of MIL-101 improves with modification: the adsorption capacity and kinetic constant are in the order of MIL-101 < ethylenediamine-grafted MIL-101 < protonated ethylenediamine-grafted MIL-101 (even though the porosity and pore size are slightly decreased with grafting and further protonation). The adsorption capacity of protonated ethylenediamine-grafted MIL-101 decreases with increasing the pH of an aqueous MO solution. These results suggest that the adsorption of MO on the MOF is at least partly due to the electrostatic interaction between anionic MO and a cationic adsorbent. Adsorption of MO at various temperatures shows that the adsorption is a spontaneous and endothermic process and that the entropy increases (the driving force of the adsorption) with MO adsorption. The adsorbent MIL-101s are re-usable after sonification in water. Based on this study, MOFs can be suggested as potential re-usable adsorbents to remove anionic dyes because of their high porosity, facile modification and ready re-activation.

1. Introduction

Recently, considerable amount of waste water having color has been generated from many industries including textile, leather, paper, printing, dyestuff, plastic and so on [1]. Removal of dye materials from water is very important because water quality is greatly influenced by color [1] and even small amount of dyes is highly visible and undesirable. Moreover, many dyes are considered to be toxic and even carcinogenic [1–3].

It is difficult to degrade dye materials because they are very stable to light and oxidation [3]. For the removal of dye materials from contaminated water, several methods such as physical, chemical and biological methods have been investigated [1,3]. Among the proposed methods, removal of dyes by adsorption technologies is regarded as one of the competitive methods because adsorption does not need a high operation temperature and several coloring materials can be removed simultaneously [1]. The versatility

of adsorption, especially with activated carbons, is due to its high efficiency, economic feasibility and simplicity of design [3].

Methyl orange (MO) is one of the well-known acidic/anionic dyes, and has been widely used in textile, printing, paper, food and pharmaceutical industries and research laboratories [2]. The structure of MO is shown in Scheme 1 and the removal of MO from water is very important due to its toxicity [2,3]. Harmful MO is selected in this study as a representative acidic dye.

Several adsorbents such as ammonium-functionalized MCM-41 and layered double hydroxides (LDH) have been studied for the removal of MO dye [4,5]. Adsorbents, including activated carbon, made from wastes attract attention to decrease the cost of adsorption [2,6]. Agricultural wastes such as lemon [7], banana and orange peel [8] and biopolymers [9] like alginate have also been used. Functionalized adsorbents such as hyper-crosslinked polymers [10] and diaminoethane sporollenin [11] have also been studied. For efficient separation of adsorbent from liquid after adsorption, magnetic particles have also been dispersed/incorporated in the adsorbent [9,12].

The thermodynamics parameters of MO adsorption have been studied over various adsorbents [2,5–7,10]. In every case, the ΔG

---

* Corresponding author. Fax: +82 53 950 6330.
  E-mail address: sung@knu.ac.kr (S.H. Jhung).
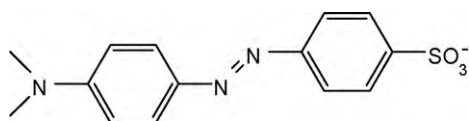
Scheme 1.

is negative for spontaneous adsorption; however ΔH depends on adsorbents [2,5–7,10] and ΔS is generally positive [2,5–7]. The adsorption kinetics has been interpreted with various models [2–10] and the adsorption of MO over MCM-41 illustrates that the adsorption process is composed of complex processes like diffusion in surface or mesopore and adsorption on mesopore [4]. Moreover, the kinetic constants vary widely depending on the adsorbents [2–10].

Metal-organic frameworks (MOFs) are crystalline porous materials which are well known for their various applications [13–20]. The particular interest in MOF materials is due to the easy tunability of their pore size and shape from a microporous to a mesoporous scale by changing the connectivity of the inorganic moiety and the nature of organic linkers [13–15]. MOFs are especially interesting in the field of adsorption, separation and storage of gases and vapors [16,19]. For example, the storage of hydrogen [16] and carbon dioxide/methane [21] using MOFs has been extensively investigated. The removal of hazardous materials such as sulfur-containing materials has also been studied [22,23].

Among the numerous MOFs reported so far, two of the most topical solids are the porous chromium-benzenedicarboxylates (Cr-BDCs) namely MIL-53 [24] (MIL stands for Material of Institute Lavoisier) and MIL-101 [25,26], which are largely studied for their potential applications. MIL-53 with a chemical formula of $Cr(OH)[C_6H_4(CO_2)_2]\cdot nH_2O$, has an orthorhombic structure and pore volume of 0.6 cc/g [24]. MIL-101, $Cr_3O(F/OH)(H_2O)_2[C_6H_4(CO_2)_2]$, has a cubic structure and huge pore volume of 1.9 cc/g [25,26]. The pore sizes of MIL-53 and MIL-101 are around 0.85 and 2.9–3.4 nm, respectively [24–26]. MIL-53 is very interesting due to the breathing effect [27], and has been widely studied for adsorption [23] and drug delivery [20,28]. MIL-101 is a very important material due to its mesoporous structure and huge porosity, and is widely studied for adsorption [29], catalysis [30] and drug delivery [20,28].

However, so far, there has been no report of the use of MOFs including Cr-BDCs in the removal of dye materials. In this work, we report, for the first time, the results of the adsorption of MO over MOFs, especially well-studied Cr-BDCs, to understand the characteristics of adsorption and possibility of using MOFs as adsorbents for the removal of dye materials from waste water.

2. Experimental

The Cr-BDCs such as MIL-53 and MIL-101 were prepared following the reported methods [24–26,31,32]. Ethylenediamine-grafted MIL-101 (ED-MIL-101) was obtained by grafting ethylenediamine according to the method reported earlier [26,30]. The protonated ED-MIL-101 (PED-MIL-101) was obtained by acidification of ED-MIL-101 with 0.1 M HCl solution at room temperature for 6 h. Activated carbon was purchased from Duksan chemical company (granule, size: 2–3 mm). The textural properties of the adsorbents were analyzed with a surface area and porosity analyzer (Micromeritics, Tristar II 3020) after evacuation at 150 °C for 12 h. The surface area, pore volume and average pore size were calculated using the nitrogen adsorption isotherms.

An aqueous stock solution of MO (1000 ppm) was prepared by dissolving MO (molecular formula: $C_{14}H_{14}N_3NaO_3S$, molecular weight: 327.34, Daejung Chemicals co. Ltd., Korea) in deionized water. Aqueous MO solutions with different concentrations of MO

(5–200 ppm) were prepared by successive dilution of the stock solution with water. The MO concentrations were determined using the absorbance (at 464 nm) of the solutions after getting the UV spectra of the solution with a spectrophotometer (Shimadzu UV spectrophotometer, UV-1800). The calibration curve was obtained from the spectra of the standard solutions (5–50 ppm) at a specific pH 5.6.

Before adsorption, the adsorbents were dried overnight under vacuum at 100 °C and were kept in a desiccator. An exact amount of the adsorbents (~10 mg) was put in the aqueous dye solutions (50 mL) having fixed dye concentrations from 20 ppm to 200 ppm. The MO solutions (pH: 5.6) containing the adsorbents were mixed well with magnetic stirring and maintained for a fixed time (10 min to 12 h) at 25 °C. After adsorption for a pre-determined time, the solution was separated from the adsorbents with a syringe filter (PTFE, hydrophobic, 0.5 μm), and the dye concentration was calculated, after dilution (if necessary), with absorbance obtained using UV spectra. The adsorption rate constant was calculated using pseudo-second or pseudo-first order reaction kinetics [33–35] and the maximum adsorption capacity was calculated using the Langmuir adsorption isotherm [33,36] after adsorption for 12 h. To get the thermodynamic parameters of adsorption such as ΔG (free energy change), ΔH (enthalpy change) and ΔS (entropy change) the adsorption was further carried out at 35 and 45 °C.

To determine the adsorption capacity at various pHs, the pH of the MO solution was adjusted with 0.1 M HCl or 0.1 M NaOH aqueous solution. The used adsorbent was activated with deionized water (0.05 g adsorbent in 25 ml water) under ultrasound (Sonics and Materials, USA; Model: VC X750, power: 750 W, amplitude; 35%) at room temperature for 60 min (temperature raised to 65 °C–70 °C after sonification). After separation, the adsorbent was dried and reused for the next adsorption.

3. Result and discussion

3.1. Adsorption kinetics

To understand the adsorption kinetics, MO was adsorbed at various times up to 12 h, and the quantity of adsorbed MO is displayed in Fig. 1 when the initial MO concentration is 30 - 50 ppm. As shown in Fig. 1, the adsorbed quantity of MO is in the order of activated carbon < MIL-53 < MIL-101 < ED-MIL-101 < PED-MIL-101 for the whole adsorption time from any initial MO concentration. The adsorbed MO slightly increases with the initial MO concentration, showing the favorable adsorption at high MO concentration. The adsorption time needed for saturation of the adsorbed amount is in the order of activated carbon > MIL-53 > MIL-101 > ED-MIL-101 > PED-MIL-101 (Supplementary data Fig. S1). The adsorption over modified MIL-101s is practically completed in 2 h, showing the rapid adsorption of MO over the modified MIL-101s. However, the adsorbed amount increases steadily with time over the activated carbon. To compare the adsorption kinetics precisely, the changes of adsorption amount with time are treated with the versatile pseudo-second-order kinetic model [33–35] because the whole data during adsorption time can be treated successfully:

$$\frac{dq_t}{dt} = k_2(q_e - q_t)^2 \tag{1}$$

$$or, \quad \frac{t}{q_t} = \frac{1}{k_2 q_e^2} + \frac{1}{q_e}t \tag{2}$$

where q_e: amount adsorbed at equilibrium (mg/g);
  q_t: amount adsorbed at time t (mg/g);
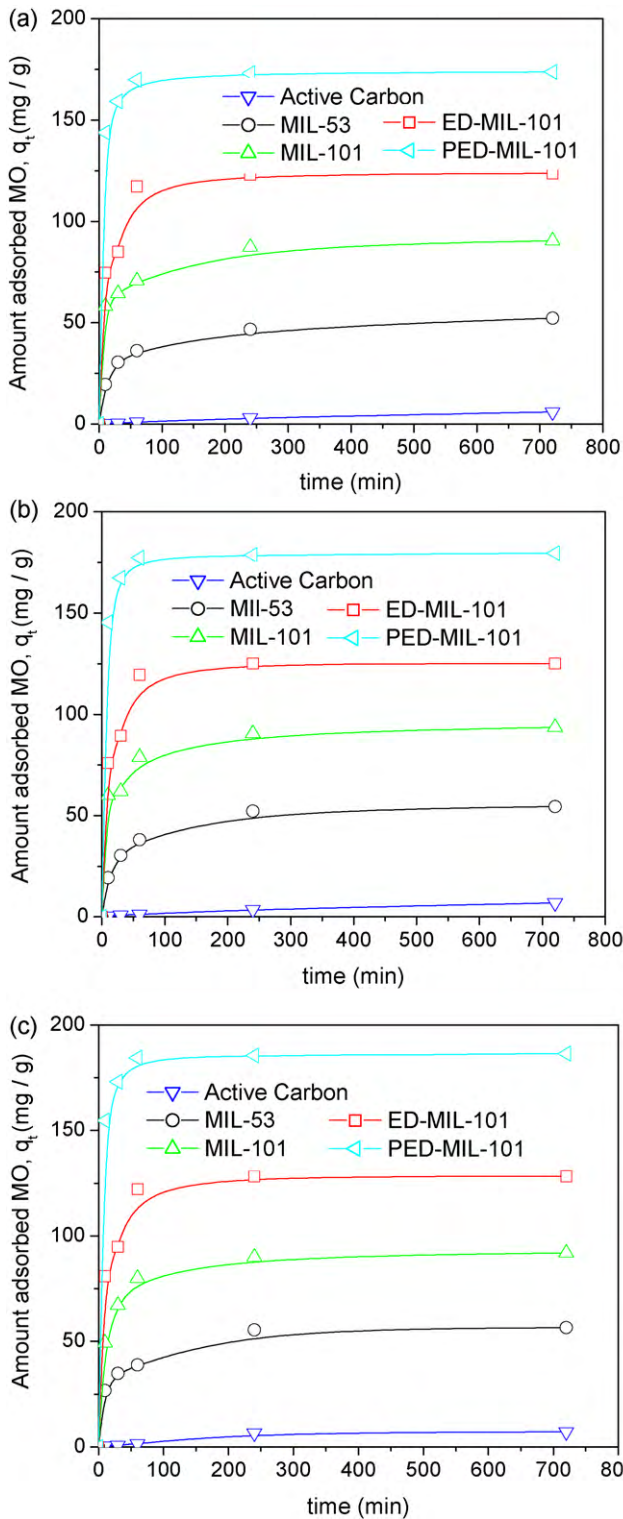 t: adsorption time (h).

Fig. 1. Effect of contact time and initial MO concentration on the adsorption of MO over the five adsorbents: (a) C_i = 30 ppm; (b) C_i = 40 ppm; (a) C_i = 50 ppm.

Fig. 2. Plots of pseudo-second-order kinetics of MO adsorption over the five adsorbents: (a) C_i = 30 ppm; (b) C_i = 40 ppm; (a) C_i = 50 ppm.

Therefore, the second-order kinetic constant (k_2) can be calculated by

$$k_2 = \frac{slope^2}{\mathrm{intercept}} \quad \text{when the } t/q_t \text{ is plotted against } t.$$

Fig. 2 shows the plots of the pseudo-second-order kinetics of the MO adsorption over the five adsorbents at three initial
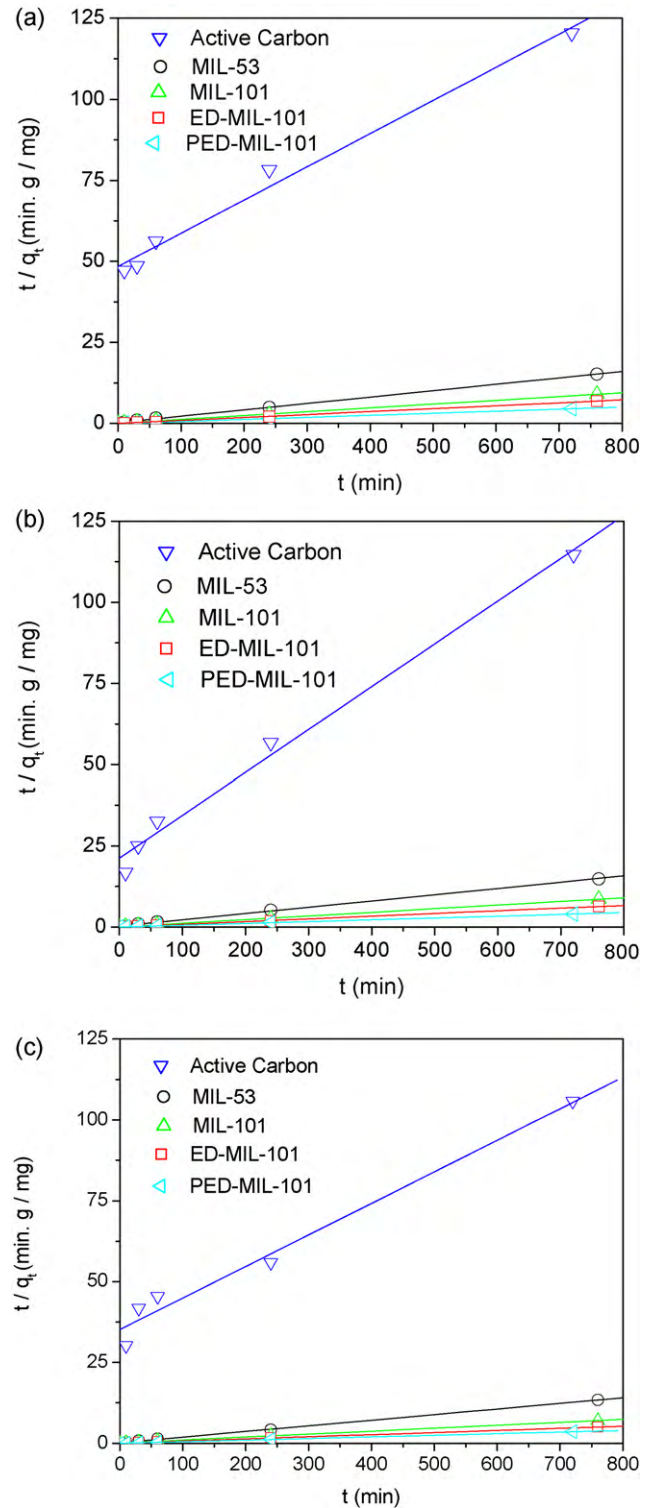
dye concentrations. The calculated kinetic constants (k_2) and correlation coefficients (R^2) are shown in Table 1. The adsorption kinetic constants for MO adsorption are in the order of activated carbon < MIL-53 < MIL-101 < ED-MIL-101 < PED-MIL-101, similar to the adsorbed quantity (Fig. 1). Therefore, PED-MIL-101 is the most effective adsorbent for MO removal in the viewpoint of adsorption amount and rate.

The adsorption kinetic constants over activated carbon and Cr-BDCs are larger than those over crosslinked polymer [10] and activated carbon (obtained from agricultural product, *Phragmites australis*) [3]. On the contrary the constants are smaller than the constants over NH_3^+-MCM-41, activated carbon (entrapping magnetic cellulose bead) [12], lemon peel [7] and alginate bead [9]. The kinetic constants over activated carbon and Cr-BDCs increase slightly with increasing the initial MO concentration, showing rapid adsorption in the presence of MO in high concentration. The increase of the kinetic constant with increasing initial adsorbate concentration has been reported too [33,37,38]. The kinetic constants of adsorption over Cr-BDCs show that the adsorption over PED-MIL-101 is the fastest and the adsorption kinetics increases with modification of virgin MIL-101. The kinetic constant over PED-MIL-101 is around 10 times greater than that of the activated carbon under the experimental conditions.

The adsorption data were also analyzed using the pseudo-first-order kinetic model [33]:

$$\ln(q_e - q_t) = \ln q_e - k_1 t \tag{3}$$

Therefore, the first order kinetic constant (k_1) can be calculated by

$k_1 = -$slope when the $\ln(q_e - q_t)$ is plotted against t.

The plots of the pseudo-first-order kinetics of the dye adsorptions over the five adsorbents at the initial MO concentrations of 30–50 ppm are shown in Fig. S2 (adsorption time is only 0–1 h for good linearity [33]) and the kinetic constants are displayed in Table S1. Similar to the second-order kinetic constants, the rate constant generally increases in the order of activated carbon < MIL-53 < MIL-101 < ED-MIL-101 < PED-MIL-101, confirming once again the most rapid adsorption over PED-MIL-101. However, the linearity of the first order kinetics is relatively poor (low correlation coefficients R^2).

The fast adsorption of MO over MIL-101, compared with the adsorption over MIL-53, is probably due to the large pore size of MIL-101 as the kinetic constant of adsorption generally increases with the increasing pore size of a porous material not only in liquid-phase adsorption [39,40] but also in gas phase adsorption [41]. However, the kinetic constants of the MIL-101s show that the pore size of the MIL-101s (Table 1) does not have any effect on the kinetics of adsorption, suggesting the presence of a specific interaction between PED-MIL-101 or ED-MIL-101 and MO because the adsorption kinetic constant increases with increasing pore size if there is no specific interaction between adsorbate and adsorbent [39–41].

3.2. Adsorption thermodynamics

The adsorption isotherms were obtained after adsorption for sufficient time of 12 h, and the results are compared in Fig. 3a. The amount of adsorbed dye is in the order of PED-MIL-101 > ED-MIL-101 > MIL-101 > MIL-53 > activated carbon for the experimental conditions, suggesting the efficiency of the Cr-BDCs, especially PED-MIL-101. As shown in Fig. 3b, the adsorption isotherms have been plotted to follow the Langmuir equation [33,36]:

$$\frac{C_e}{q_e} = \frac{C_e}{Q_0} + \frac{1}{Q_0 b} \tag{4}$$

where C_e: equilibrium concentration of adsorbate (mg/L)

q_e: the amount of adsorbate adsorbed (mg/g)

Q_0: Langmuir constant (maximum adsorption capacity) (mg/g)

b: Langmuir constant (L/mg or L/mol)

So, the Q_0 can be obtained from the *reciprocal of the slope* of a plot of C_e/q_e against C_e.

The Q_0 for all of the samples is determined from Fig. 3b and the values are summarized in Table 1. Generally the Q_0 increases in the
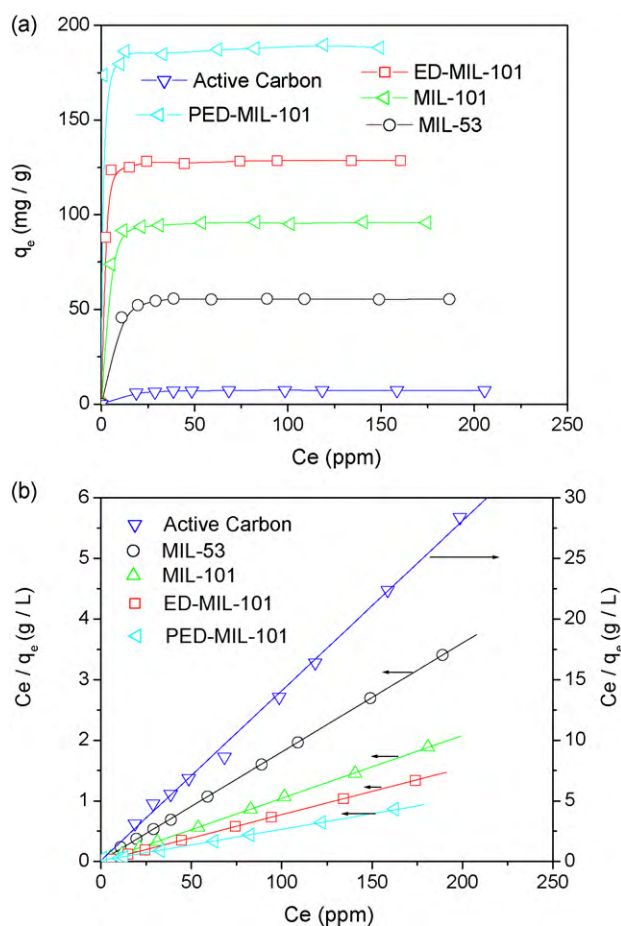

Fig. 3. (a) Adsorption isotherms for MO adsorption over the five adsorbents and (b) Langmuir plots of the isotherms (a). The arrows in (b) show that the y-axis scale of activated carbon is different to that of MOFs.

order of activated carbon < MIL-53 < MIL-101 < ED-MIL-101 < PED-MIL-101, and the adsorption capacity of PED-MIL-101 is 194 mg/g. The large adsorption capacity of MIL-101 for MO, compared to that of MIL-53, is probably due to the large porosity of MIL-101 as the adsorption capacity generally increases with increasing the porosity of adsorbents [42,43].

So far many adsorbents have been evaluated as candidates for the removal of MO from water and their adsorption capacities have varied widely from 2.1 to about 366 mg/g depending on the adsorbent [1–12]. Even though the adsorption capacity of Cr-BDCs is less than that of NH_3^+-MCM-41 [4], LDH [5] and activated carbon (made from an agricultural product, *Phragmites australis*) [3], its capacity is relatively greater than that of the most adsorbents [1,2,6–12].

To shed light on the MO adsorption over Cr-BDCs, the adsorption free energy, enthalpy and entropy change were calculated from the adsorption of MO over PED-MIL-101 at various temperatures. Fig. 4a shows the adsorption isotherms at the temperature of 25, 35 and 45 °C, and the Langmuir plots are displayed in Fig. 4b. The adsorption capacity increases with increasing adsorption temperature, suggesting endothermic adsorption.

The Gibbs free energy change ΔG can be calculated by the following Eq. (5) [5,6,10,35]:

$$\Delta G = -RT \ln b \tag{5}$$

(where R is the gas constant)

The Langmuir constant b (dimension: L/mol) can be obtained from the *slope/intercept* of the Langmuir plot of Fig. 4b. The negative free energy change (ΔG) shown in Table 2 suggests spontaneous adsorption under the adsorption conditions.
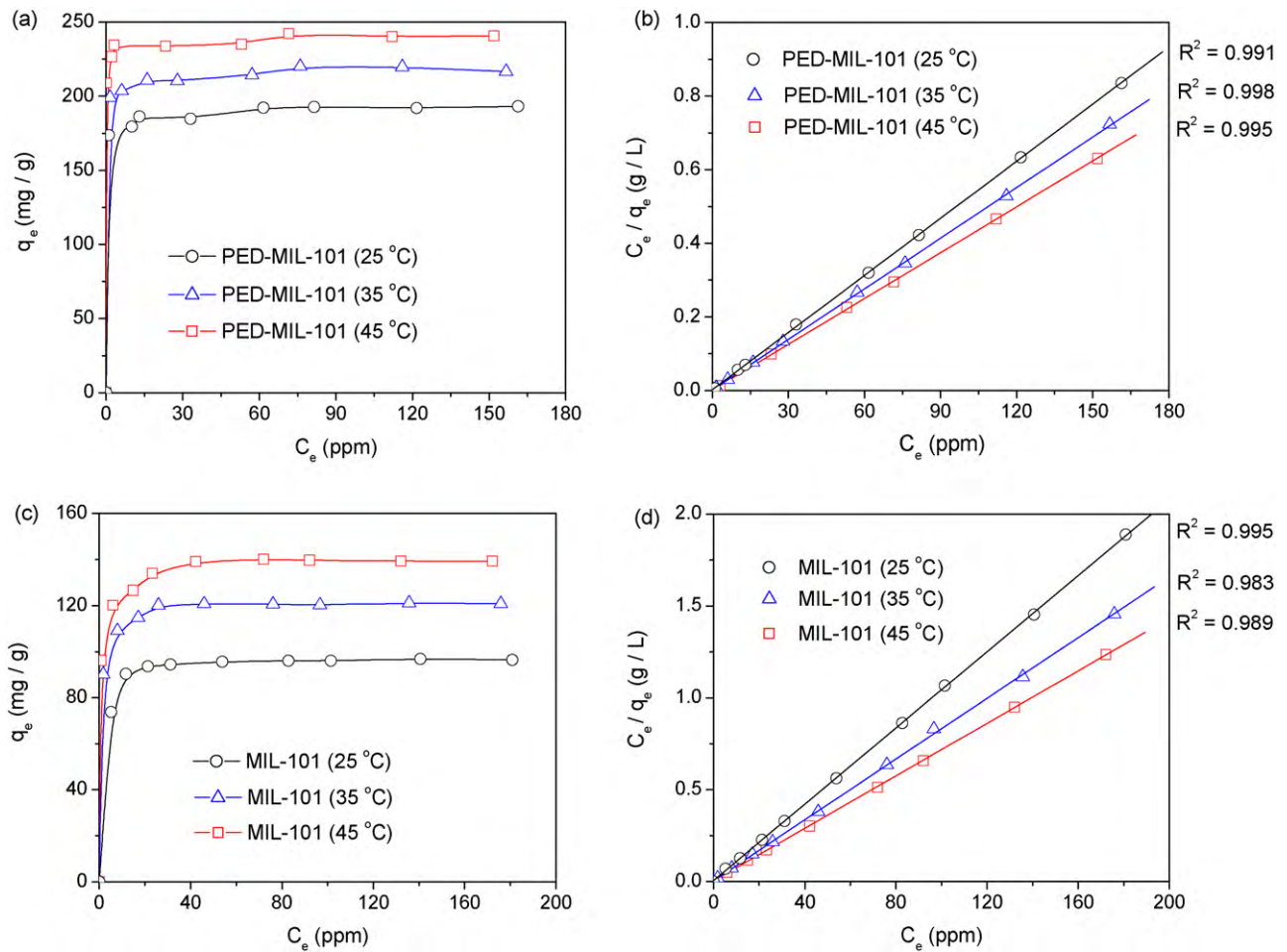
Fig. 4. (a) Adsorption isotherms for MO adsorption over PED-MIL-101 at 25, 35 and 45 °C; and (b) Langmuir plots of the isotherms (a); (c) Adsorption isotherms for MO adsorption over MIL-101 at 25, 35 and 45 °C; and (d) Langmuir plots of the isotherms (c).

The enthalpy change ΔH can be obtained by using the van't Hoff equation [5,44]:

$$\ln b = \frac{\Delta S}{R} - \frac{\Delta H}{RT} \tag{6}$$

The calculated ΔH, obtained from the $(-slope \times R)$ of the van't Hoff plot (Fig. 5), is 29.5 kJ/mol, confirming endothermic adsorption in accord with the increasing adsorption capacity associated with increasing adsorption temperature (Fig. 4a). The endothermic

Table 1
Textural properties, the pseudo-second-order kinetic constants (k^2) with correlation constants (R^2) at various MO concentrations and the maximum adsorption capacities (Q_0) of the five adsorbents.

Adsorbent (pore size, nm)	BET surface area (m²/g)	Total pore volume (cm³/g)	Pseudo-second-order kinetics constants k_2 (g/(mg min))						Maximum adsorption capacity, Q_o (mg/g)
			30 ppm		40 ppm		50 ppm		
			k_2	R^2	k_2	R^2	k_2	R^2	
Activated carbon (<1.0)	1068	0.50	2.17×10^{-4}	0.987	2.34×10^{-4}	0.981	2.59×10^{-4}	0.978	11.2
MIL-53 (<1.0)	1438	0.55	7.23×10^{-4}	0.999	7.70×10^{-4}	0.999	7.84×10^{-4}	0.999	57.9
MIL-101 (1.6, 2.1)	3873	1.70	9.01×10^{-4}	0.999	9.19×10^{-4}	0.996	9.29×10^{-4}	0.999	114
ED-MIL-101 (1.4, 1.8)	3491	1.37	1.06×10^{-3}	0.998	1.19×10^{-3}	0.999	1.27×10^{-3}	0.999	160
PED-MIL-101 (1.4, 1.8)	3296	1.18	2.75×10^{-3}	1.00	2.95×10^{-3}	1.00	3.04×10^{-3}	0.999	194

Table 2
The maximum adsorption capacity and thermodynamic parameters of MO adsorption over PED-MIL-101 and MIL-101 at different temperatures.

Adsorbent	Temp. (°C)	Q_o (mg/g)	ΔG (kJ/mol)	ΔH (kJ/mol)	ΔS (J/mol/K)
PED-MIL-101	25	194	−32.5		
	35	219	−34.5	29.5	209
	45	241	−36.6		
MIL-101	25	114	−31.9		
	35	121	−33.1	4.00	120
	45	140	−34.3		

Table 3
The equilibrium adsorbed amount (q_e) and pseudo-second-order kinetic constant (k_2) of fresh and reused PED-MIL-101s and ED-MIL-101s (Temperature: 25 °C, C_i: 50 ppm).

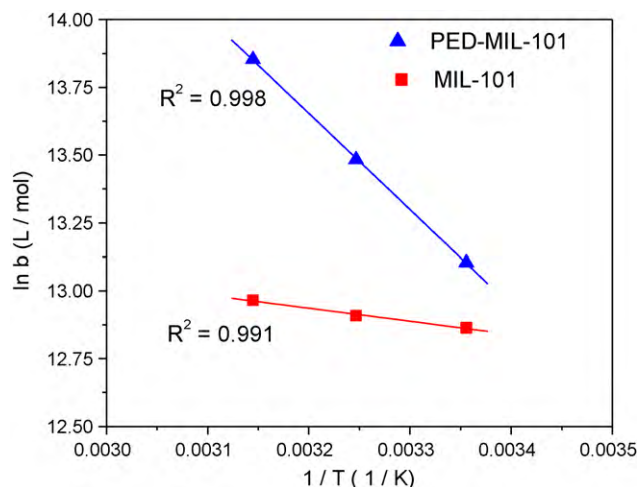| Adsorbent	Items	Fresh	1st reuse	2nd reuse
PED-MIL-101	q_e (mg/g)	187	186	181
	k_2 (g/mg min)	3.04×10^{-3}	1.87×10^{-3}	1.18×10^{-3}
ED-MIL-101	q_e (mg/g)	130	127	123
	k_2 (g/mg min)	1.27×10^{-3}	1.07×10^{-3}	7.62×10^{-4}

Fig. 5. van't Hoff plots to get the ΔH and ΔS of the MO adsorption over the MIL-101 and PED-MIL-101.

adsorption may be due to a stronger interaction between pre-adsorbed water and the adsorbent than the interaction between MO and the adsorbent. However, further work is necessary to clarify this suggestion.

The entropy change ΔS can be obtained from the ($intercept \times R$) of the van't Hoff plot (Fig. 5), and the obtained entropy change ΔS is 208 J/(mol K). The positive ΔS means the increased randomness with adsorption of MO probably because the number of desorbed water molecule is larger than that of the adsorbed MO molecule (MO is very bulky compared with water; therefore several water may be desorbed by adsorption of a MO molecule). Therefore, the driving force of MO adsorption (negative ΔG) on PED-MIL-101 is due to an entropy effect (large positive ΔS) rather than an enthalpy change (ΔH is positive).

The thermodynamic properties were also determined for the case of MIL-101 using the adsorption isotherms (Fig. 4c) and the Langmuir plots at different temperatures (Fig. 4d). Generally, the isotherms and Langmuir plots are similar to those of PED-MIL-101 (Fig. 4a and b). However, it should be mentioned that the adsorbed amount of MO over PED-MIL-101 is high at very low concentration (especially at 45 °C), which is very helpful to remove MO even at a low concentration. The adsorption free energy, enthalpy and entropy change over MIL-101, obtained from Fig. 4d and Fig. 5, are displayed in Table 2. Similar to PED-MIL-101, the adsorption of MO over MIL-101 is a spontaneous process (negative ΔG). However, the absolute value of ΔH is very small for the case of MIL-101. This may be due to a physical adsorption of MO and little desorption of pre-adsorbed water. The small free energy change (ΔS) supports this assumption (small number of desorbed water molecules). However, a more detailed study will be necessary to understand the difference between MIL-101 and PED-MIL-101 in terms of the adsorption enthalpy and entropy changes.

3.3. Effect of pH and regeneration of MOFs

The adsorption of a dye usually highly depends on the pH of the dye solution [2,6]. MO adsorption at various pH values was measured after equilibration with PED-MIL-101 and activated carbon. As shown in Fig. 6, the adsorbed amounts decrease with increasing the pH of the MO solution, which is quite similar to previously reported results [2,6]. The decreasing of adsorbed MO with increasing pH might be due to the fact that the concentration of positive charge of adsorbents is decreased with increasing pH.
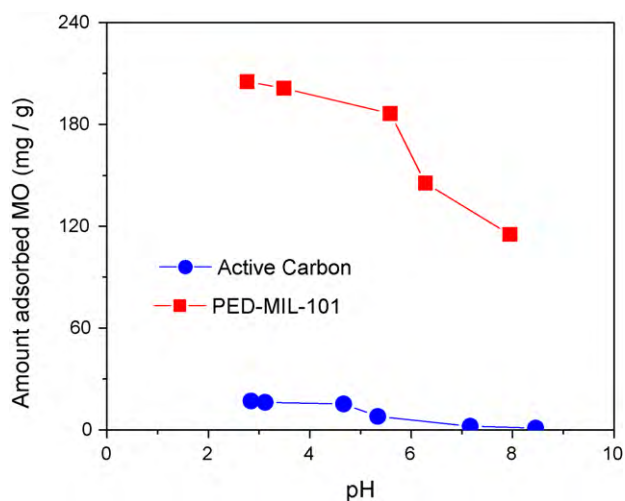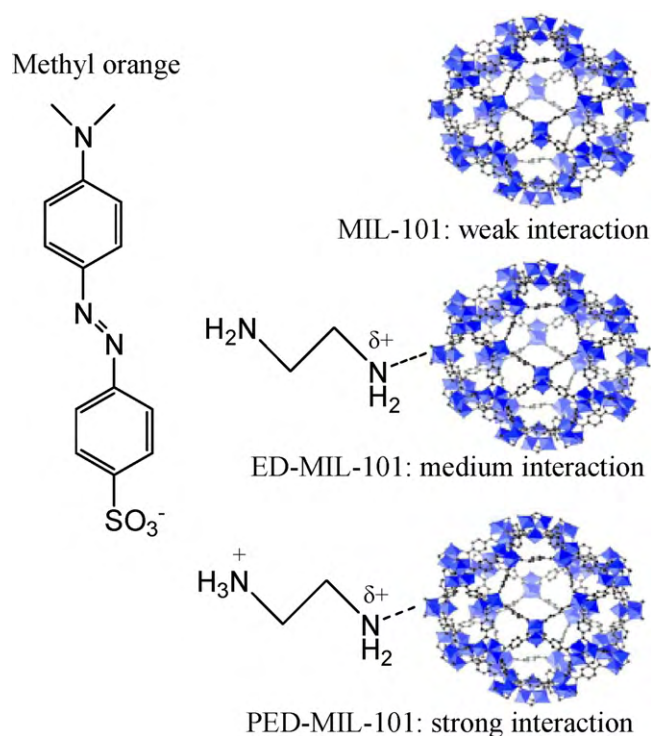

Fig. 6. Effect of pH of MO solution on the adsorbed amount of MO over activated carbon and PED-MIL-101 (C_i: 50 ppm, adsorption time: 4 h).
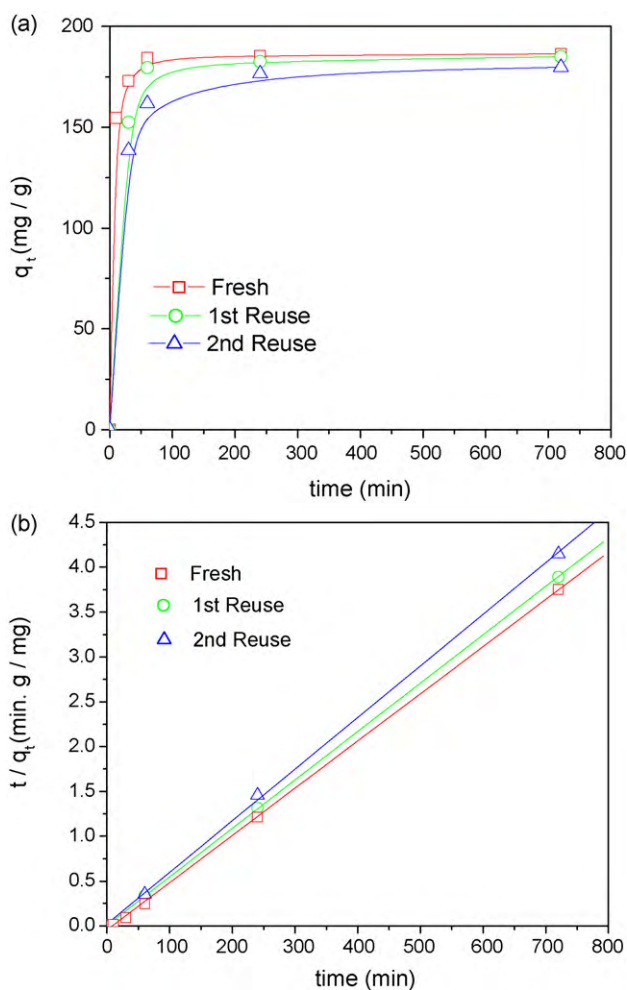

Scheme 2.

Fig. 7. (a) Effect of contact time on the MO adsorption and (b) Pseudo-second-order plots to show the re-usability of the spent PED-MIL-101.

Even though more detailed work is necessary to clearly understand the mechanism of MO adsorption on Cr-BDCs, the mechanism may be explained with electrostatic interaction between MO and adsorbents (as proposed in Scheme 2). MO usually exists in the sulfate form; therefore, there will be a strong electrostatic interaction with an adsorbent having a positive charge. The positive charge distribution increases in the order of MIL-101 < ED-MIL-101 < PED-MIL-101 as suggested in Scheme 2. On the other hand the positive charge of PED-MIL-101 will be decreased with increasing the pH of the solution due to the deprotonation of the protonated adsorbent. Therefore, the increase of adsorption capacity and kinetic constant with modification (MIL-101 < ED-MIL-101 < PED-MIL-101) or increasing acidity may be explained with the increased positive charge of the adsorbent, especially PED-MIL-101 in a low pH condition. A similar adsorption mechanism of anionic dyes *via* electrostatic interaction has been reported in the case of chitosan [44] and NH_3^+-MCM-41 [4].

Facile regeneration of an adsorbent is very important for commercial feasibility. The re-usability of spent adsorbent (PED-MIL-101) is shown in Fig. 7a. Even though the adsorption kinetic constants (shown in Table 3 which are derived from Fig. 7b) decrease noticeably with the cycle of adsorption, the amount of adsorbed MO does not decrease much, suggesting the applicability of Cr-BDCs in the adsorptive removal of anionic dye materials from waste water. Similar re-usability of ED-MIL-101 has also been observed (Table 3, Supporting Fig. 3).

4. Conclusion

The liquid-phase adsorption of MO over MOF-type materials has been studied to understand the characteristics of dye adsorption on these materials. The adsorption capacity and adsorption kinetic constant of MIL-101 are greater than those of MIL-53, showing the importance of porosity and pore size for adsorption, which is similar to reported results. MIL-101, after being modified to have a positive charge, can be efficiently used to remove MO *via* liquid-phase adsorption. Based on the rate constant (pseudo-second or pseudo-first-order kinetics for adsorption) and adsorption capacity, it can be suggested that there is a specific interaction like electrostatic interaction between MO and the adsorbent for rapid and high uptake of the dye. The adsorption of MO over PED-MIL-101 at various temperatures shows that the adsorption is spontaneous and endothermic and the randomness increases with the adsorption of MO. The driving force of MO adsorption over PED-MIL-101 is mainly due to an entropy effect rather than an enthalpy change. From this study, it can be suggested that the MOF-type materials may be applied in the regenerable adsorptive removal of anionic dye materials from contaminated water.

Acknowledgements

Appendix A. Supplementary data

Supplementary data associated with this article can be found, in the online version, at doi:10.1016/j.jhazmat.2010.05.047.

References

[1] G. Crini, Non-conventional low-cost adsorbents for dye removal: a review, Bioresour. Technol. 97 (2006) 1061–1085.
[2] A. Mittal, A. Malviya, D. Kaur, J. Mittal, L. Kurup, Studies on the adsorption kinetics and isotherms for the removal and recovery of Methyl Orange from wastewaters using waste materials, J. Hazard. Mater. 148 (2007) 229–240.
[3] S. Chen, J. Zhang, C. Zhang, Q. Yue, Y. Li, C. Li, Equilibrium and kinetic studies of methyl orange and methyl violet adsorption on activated carbon derived from *Phragmites australis*, Desalination 252 (2010) 149–156.
[4] Q. Qin, J. Ma, K. Liu, Adsorption of anionic dyes on ammonium-functionalized MCM-41, J. Hazard. Mater. 162 (2009) 133–139.
[5] Z.-M. Ni, S.-J. Xia, L.-G. Wang, F.-F. Xing, G.-X. Pan, Treatment of methyl orange by calcined layered double hydroxides in aqueous solution: adsorption property and kinetic studies, J. Colloid Interface Sci. 316 (2007) 284–291.
[6] K.P. Singh, D. Mohan, S. Sinha, G.S. Tondon, D. Gosh, Color Removal from Wastewater Using Low-Cost Activated Carbon Derived from Agricultural Waste Material, Ind. Eng. Chem. Res. 42 (2003) 1965–1976.
[7] A. Bhatnagar, E. Kumar, A.K. Minocha, B.-H. Jeon, H. Song, Y.-C. Seo, Removal of anionic dyes from water using Citrus limonum (lemon) peel: equilibrium studies and kinetic modeling, Sep. Sci. Technol. 44 (2009) 316–334.
[8] G. Annadurai, R.-S. Juang, D.-J. Lee, Use of cellulose-based wastes for adsorption of dyes from aqueous solutions, J. Hazard. Mater. 92 (2002) 263–274.
[9] V. Rocher, J.-M. Siaugue, V. Cabuil, A. Bee, Removal of organic dyes by magnetic alginate beads, Water Res. 42 (2008) 1290–1298.
[10] J.-H. Huang, K.-L. Huang, S.-Q. Liu, A.-T. Wang, C. Yan, Adsorption of rhodamine B and methyl orange on a hypercrosslinked polymeric adsorbent in aqueous solution, Colloid Surf. A: Physicochem. Eng. Aspects 330 (2008) 55–61.
[11] A. Ayar, O. Gezici, M. Küçükosmanoğlu, Adsorptive removal of methylene blue and methyl orange from aqueous media by carboxylated diaminoethane sporopollenin: on the usability of an aminocarboxilic acid functionality-bearing solid-stationary phase in column techniques, J. Hazard. Mater. 146 (2007) 186–193.
[12] X. Luo, L. Jhang, High effective adsorption of organic dyes on magnetic cellulose beads entrapping activated carbon, J. Hazard. Mater. 171 (2009) 340–347.
[13] G. Férey, Hybrid porous solids: past, present, future, Chem. Soc. Rev. 37 (2008) 191–214.
[14] S. Kitagawa, R. Kitaura, S.-I. Noro, Functional porous coordination polymers, Angew. Chem. Int. Ed. 43 (2004) 2334–2375.
[15] O.M. Yaghi, M. O'Keeffe, N.W. Ockwig, H.K. Chae, M. Eddaoudi, J. Kim, Reticular synthesis and the design of new materials, Nature 423 (2003) 705–714.

[16] L.J. Murray, M. Dincă, J.R. Long, Hydrogen storage in metal-organic frameworks, Chem. Soc. Rev. 38 (2009) 1294–1314.

[17] D. Farrusseng, S. Aguado, C. Pinel, Metal-organic frameworks: opportunities for catalysis, Angew. Chem. Int. Ed. 48 (2009) 7502–7513.

[18] J. Lee, O.K. Farha, J. Roberts, K.A. Scheidt, S.T. Nguyen, J.T. Hupp, Metal-organic framework materials as catalysts, Chem. Soc. Rev. 38 (2009) 1450–1459.

[19] J.-R. Li, R.J. Kuppler, H.-C. Zhou, Selective gas adsorption and separation in metal-organic frameworks, Chem. Soc. Rev. 38 (2009) 1477–1504.

[20] P. Horcajada, C. Serre, G. Maurin, N.A. Ramsahye, F. Balas, M. Vallet-Regí, M. Sebban, F. Taulelle, G. Férey, Flexible porous metal-organic frameworks for a controlled drug delivery, J. Am. Chem. Soc. 130 (2008) 6774–6790.

[21] P.L. Llewellyn, S. Bourrelly, C. Serre, A. Vimont, M. Daturi, L. Hamon, G. De Weireld, J.-S. Chang, D.Y. Hong, Y.K. Hwang, S.H. Jhung, G. Férey, High uptakes of CO_2 and CH_4 in the mesoporous metal-organic-frameworks MIL-100 and MIL-101, Langmuir 24 (2008) 7245–7250.

[22] K.A. Cychosz, A.G. Wong-Foy, A.J. Matzger, Liquid phase adsorption by microporous coordination polymers: removal of organosulfur compounds, J. Am. Chem. Soc. 130 (2008) 6938–6939.

[23] L. Hamon, C. Serre, T. Devic, T. Loiseau, F. Millange, G. Férey, G.D. Weireld, Comparative study of hydrogen sulfide adsorption in the MIL-53(Al, Cr, Fe), MIL-47(V), MIL-100(Cr), and MIL-101(Cr) metal-organic frameworks at room temperature, J. Am. Chem. Soc. 131 (2009) 8775–8777.

[24] C. Serre, F. Millange, C. Thouvenot, M. Noguès, G. Marsolier, D. Louër, G. Férey, Very large breathing effect in the first nanoporous chromium(III)-based solids: MIL-53 or $Cr^{III}(OH) \cdot \{O_2C-C_6H_4-CO_2\} \cdot \{HO_2C-C_6H_4-CO_2H\}x \cdot H_2Oy$, J. Am. Chem. Soc. 124 (2002) 13519–13526.

[25] G. Férey, C. Mellot-Draznieks, C. Serre, F. Millange, J. Dutour, S. Surble, I. Mirgiolaki, A chromium terephthalate-based solid with unusually large pore volumes and surface area, Science 309 (2005) 2040–2042.

[26] D.-Y. Hong, Y.K. Hwang, C. Serre, G. Férey, J.-S. Chang, Porous chromium terephthalate MIL-101 with coordinatively unsaturated sites: surface functionalization, encapsulation, sorption and catalysis, Adv. Funct. Mater. 19 (2009) 1537–1552.

[27] C. Serre, C. Mellot-Draznieks, S. Surblé, N. Audebrand, Y. Filinchuk, G. Férey, Role of solvent–host interactions that lead to very large swelling of hybrid frameworks, Science 315 (2007) 1828–1831.

[28] P. Horcajada, C. Serre, M. Vallet-Regi, M. Sebban, F. Taulelle, G. Ferey, Metal-organic frameworks as efficient materials for drug delivery, Angew. Chem. Int. Ed. 45 (2006) 5974–5978.

[29] M. Latroche, S. Surblé, C. Serre, C. Mellot-Draznieks, P.L. Llewellyn, J.-H. Lee, J.-S. Chang, S.H. Jhung, G. Férey, Hydrogen storage in the giant-pore metal-organic frameworks MIL-100 and MIL-101, Angew. Chem. Int. Ed. 45 (2006) 8227–8231.

[30] Y.K. Hwang, D.-Y. Hong, J.-S. Chang, S.H. Jhung, Y.-K. Seo, J. Kim, A. Vimont, M. Daturi, C. Serre, G. Férey, Amine grafting on coordinatively unsaturated metal centers of MOFs: consequences for catalysis and metal encapsulation, Angew. Chem. Int. Ed. 47 (2008) 4144–4148.

[31] N.A. Khan, S.H. Jhung, Phase-transition and phase-selective synthesis of porous chromium-benzenedicarboxylates, Cryst. Growth Des. 10 (2010) 1860–1865.

[32] N.A. Khan, J.W. Jun, S.H. Jhung, Effect of water concentration and acidity on the synthesis of porous chromium benzenedicarboxylates, Eur. J. Inorg. Chem. (2010) 1043–1048.

[33] B.H. Hameed, A.A. Rahman, Removal of phenol from aqueous solutions by adsorption onto activated carbon prepared from biomass material, J. Hazard. Mater. 160 (2008) 576–581.

[34] Y.S. Ho, G. McKay, Pseudo-second order model for sorption processes, Process Biochem. 34 (1999) 451–465.

[35] S. Wang, H. Li, L. Xu, Application of zeolite MCM-22 for basic dye removal from wastewater, J. Colloid Interface Sci. 295 (2006) 71–78.

[36] S.-H. Lin, R.-S. Juang, Adsorption of dye and its derivatives from water using synthetic resins and low-cost natural adsorbents: a review, J. Environ. Manag. 90 (2009) 1336–1349.

[37] A.T.M. Din, B.H. Hameed, A.L. Ahmad, Batch adsorption of phenol onto physiochemical-activated coconut shell, J. Hazard. Mater. 161 (2009) 1522–1529.

[38] V.C. Srivastava, M.M. Swamy, I.D. Mall, B. Prasad, I.M. Mishra, Adsorptive removal of phenol by bagasse fly ash and activated carbon: equilibrium, kinetics and thermodynamics, Colloid Surf. A 272 (2006) 89–104.

[39] D.P. Xu, S.-H. Yoon, I. Mochida, W.M. Qiao, Y.G. Wang, L.C. Ling, Synthesis of mesoporous carbon and its adsorption property to biomolecules, Micropor. Mesopor. Mater. 115 (2008) 461–468.

[40] S.H. Jhung, J.-H. Lee, J.W. Yoon, C. Serre, G. Férey, J.-S. Chang, Microwave synthesis of chromium terephthalate MIL-101 and its benzene sorption ability, Adv. Mater. 19 (2007) 121–124.

[41] S.H. Jhung, H.-K. Kim, J.W. Yoon, J.-S. Chang, Low-temperature adsorption of hydrogen on nanoporous aluminophosphates: effect of pore size, J. Phys. Chem. B 110 (2006) 9371–9374.

[42] V. Fierro, V. Torné-Fernández, D. Montané, A. Celzard, Adsorption of phenol onto activated carbons having different textural and surface properties, Micropor. Mesopor. Mater. 111 (2008) 276–284.

[43] E. Haque, N.A. Khan, S.N. Talapaneni, A. Vinu, S.H. Jhung, Adsorption of phenol on mesoporous carbon CMK-3: effect of textural properties, Bull. Korean Chem. Soc. (2010), in press.

[44] G. Crini, P.-M. Badot, Application of chitosan, a natural aminopolysaccharide, for dye removal from aqueous solutions by adsorption processes using batch studies: a review of recent literature, Prog. Polym. Sci. 33 (2008) 399–447.